ECS Transactions, 57 (1) 1175-1184 (2013)
10.1149/05701.1175ecst ©The Electrochemical Society

Full Ceramic Fuel Cells Based on Strontium Titanate Anodes, An Approach Towards More Robust SOFCs

P. Holtappels[a], J.T.S. Irvine[b], B. Iwanschitz[c], L. Theil Kuhn[a], L. Y. Lu[b], Q. Ma[d], J. Malzbender[d], A. Mai[c], T. Ramos[a], J. Rass-Hansen[f], B. R. Sudireddy[a], F. Tietz[d], V. Vasechko[d], S. Veltzé[a], M.C. Verbraeken[b]

[a] Department of Energy Conversion, Technical University of Denmark, DK-4000, Roskilde Denmark
[b] School of Chemistry, University of St Andrews, St Andrews Fife KY16 9ST, United Kingdom
[c] Hexis AG, Winterthur, Switzerland
[d] Institute for Energy and Climate, Forschungszentrum Jülich, 52425 Jülich , Germany
[f] Topsoe Fuel Cell A/S, 2800 Kgs Lyngby, Denmark

The persistent problems with Ni-YSZ cermet based SOFCs, with respect to redox stability and tolerance towards sulfur has stimulated the development of a full ceramic cell based on strontium titanate(ST)- based anodes and anode support materials, within the EU FCH JU project SCOTAS-SOFC. Three different compositions (La, Y and Nb substituted ST) have been developed as anode backbones for either 25 cm^2 or larger than 100 cm^2 cell areas. Cell performances, once infiltrated with suitable electro catalysts, exhibited a maximum power density of 0.5 W/cm^2 at 850 °C. While the ST based backbone remains intact and tolerant to redox cycles, cell performance degradation appears linked to the infiltrated electro catalysts. The materials have also been assessed with respect to their electrical and mechanical properties, in order to further evaluate their potential use as anode and anode support layers in SOFCs.

Introduction

Solid oxide fuel cells (SOFCs) have a great advantage in their fuel flexibility compared to other fuel cells (such as PEMFCs) thus particularly suited for stationary co-generation of heat and power based on natural gas or other hydrocarbon fuels. However, the Ni-cermet, the state-of-the-art SOFC anode, suffers from several limitations, namely limited tolerance to re-oxidation, sensitivity to sulfur poisoning and coking. These limitations have been, to date, handled on the system level, and especially for small scale, combined heat and power systems (micro CHP), increase the system complexity, since both cell and stack must be protected during critical operation stages, e.g. Start Up/Shut down (redox stability, C tolerance required) and Grid outage/system failures (redox, sulfur, C-tolerance required).

Within the frame of the European Fuel Cell and Hydrogen Joint Undertaking, the SCOTAS-SOFC project aims at demonstrate a more robust SOFC anode, replacing the

common porous Ni-Cermet with an alternative ceramic material. Based on previous work, three strontium titanate (ST) compositions have been identified, and are currently being further developed for integration into full cell stacks, with cell areas up to 144 cm^2 , to be evaluated under micro CHP relevant operation conditions. So being, SCOTAS-SOFC is aiming to the following targets for stationary fuel cells: 45 % electrical efficiency, 80 % CHP efficiency and increased fuel flexibility.

Concept and Experimental Details

The current approach is based on a porous ST-based ceramic backbone, which is then infiltrated with a metal salt solution, or a suitable combination of solutions, to form suitable nano-sized electrocatalyst particles after thermal decomposition (1). Based on a detailed review of previous results (2), three ST systems have been selected. The selected compositions, synthesis and forming methods are given in TABLE I. The materials have also been characterized with respect to the influence of fabrication conditions and porosity on their electrical conductivity and mechanical stability.

TABLE I. Strontium titanate compositions and forming procedures

Material	Composition	Powder Synthesis	Anode /support fabrication method	Pre-treatment S: Sintering R: Pre-reduction
LSCT	$La_{0.20}Sr_{0.35}Ca_{0.45}TiO_3$	Drip pyrolysis	Tape casting	S: 1250 - 1300 °C (air) R: None
LST	$Sr_{0.7}La_{0.2}TiO_3$	Spray drying and calcination	Warm pressing	S: 1350 - 1400 °C (air) R: 1100 - 1200 °C (4%H_2)
SYT	$Sr_{0.895}Y_{0.07}TiO_3$	Spray drying and calcination	Warm pressing	S: 1350 - 1400 °C (4%H_2) R: None
STN	$Sr_{0.94}Ti_{0.9}Nb_{0.1}O_3$	Solid state synthesis	Screen printing/ tape casting	S: 1225 - 1275 °C (air) R: None

Anode layers have been benchmarked as button cells and full cells in electrolyte supported (ESC) and anode supported (ASC) designs. ESCs have been prepared and tested as 25 cm^2 and 100 cm^2 sized cells. The active area of the 25 cm^2 cells is 16 cm^2. ASCs have been developed up to 144 cm^2 areas however, successful tests are up to now limited to button cells and 25 cm^2 sized cells.

Cell testing for all cells include electrochemical impedance spectroscopy (EIS), iV characteristics and time dependent measurements under constant current, in a temperature range from 650 to 900 °C. The fuels were either H_2/H_2O ($H_2O \leq 50$ %) or CPOX reformate. Further details concerning testing parameters will be given where appropriate.

Results and Discussion

Electrical Conductivity of Porous Structures

The electrical conductivity of two different ST-systems, STN and LSCT based - was measured at 900 °C, over 1000 hours, and can be seen in Figure 1. In general, all porous ST structures have lower electrical conductivity, when compared to the dense material and state of the art Ni-cermet anodes (> 400 S/cm). However, it appears that the LSCT

has a higher electrical conductivity then STN. All samples revealed an activation phase, corresponding to a large conductivity increase, shortly after the introduction of H_2/N_2, which lasted for approximately 70 hours. Afterwards, the electrical conductivity only slightly increased. Moreover, redox-cycling (2 hours reoxoduiase in air) not only did not negatively influence the electrical conductivity of any of the studied ST-systems, it in fact introduced a new activation phase upon re-reduction, increasing the previously attained conductivity values. The results indicate that the reduction of the anodes is a rather slow process. However, with the requirement of SOFC operation times above 40,000 hours for micro-CHP systems, longer reduction times are not considered critical The electrical conductivity of STs in reducing atmospheres largely depends on the reduction kinetics, and thus on the pre-treatment of the materials. In this particular case, neither STN nor LSCT had suffered any pre-reduction treatment, and thus the higher conductivity exhibited by LSCT may be attributed to faster reduction kinetics. However, microstructure and/or fabrication procedure cannot not be excluded, at this point, as additional contributors to the very low total conductivities obtained for these porous structures, as well as to the differences in conductivity between STN and LSCT systems. It should be mentioned that a significantly lower lateral conductivity has also recently been reported for LSM cathodes, which cannot be attributed to porosity but rather to segregation within the grain boundaries (3).

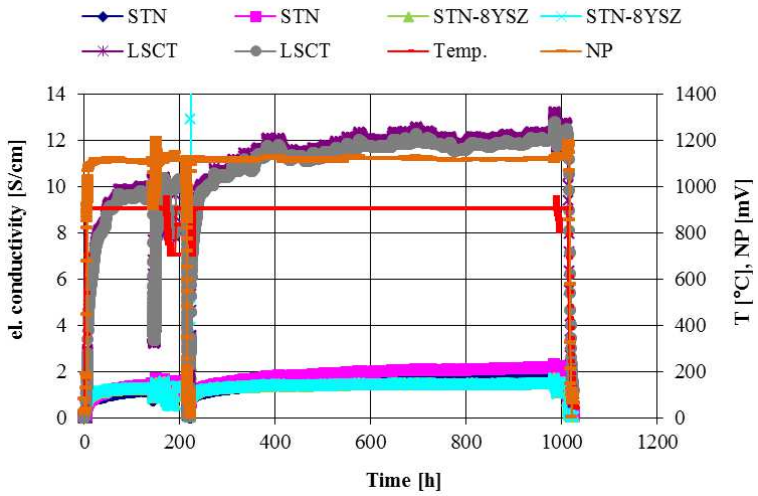

Figure 1. 4-point conductivity of STN-based and LSCT thin films in H_2/N_2 atmosphere at 900°C. test conditions e.g.temperature (Temp) and Nernst potential (NP) are stable over the whole testing period.

Mechanical Stability of Porous Structures

The mechanical robustness of the ceramic substrate is an important aspect to ensure long-term, reliable operation of a SOFC stack. Investigations of the mechanical properties of SYT-, LSCT- and STN materials was performed in the as-sintered state. Room temperature micro-indentation allowed the determination of Young's modulus and hardness, whereas the temperature dependence of the Young's modulus was measured with the impulse excitation technique, up to ~ 950 °C. Since high porosity is vital for anode materials, the effective porosity dependence of the Young's modulus was measured and compared to strength data from (4). Post-test fractographic analysis was also performed using stereo-, confocal and scanning electron microscopy (not shown)

which revealed important information on fracture origins and critical defects in the material. Details on the experimental methods can be found in (5).

Figure 2 shows the Young's modulus dependence on temperature. Reflected on the measured values are the different porosities. The complex temperature behaviors for SYT and LSCT were completely reversible. The temperature dependence of strength agrees with the Young's modulus data normalized to the room temperature value. Initial results suggest that with respect to creep SYT is superior to Ni-YSZ cermets.

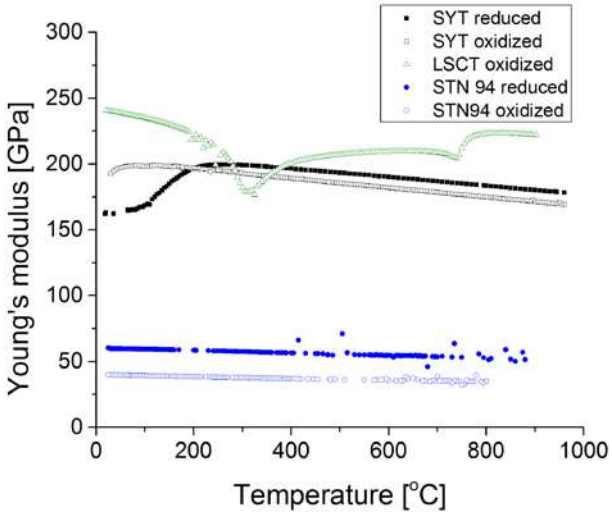

Figure 2. Young's modulus - temperature dependency for the three ST-systems in both reduced and oxidised conditions.

Figure 3 compares the Young's modulus against strength data for SYT only, revealing the existence of a similar porosity dependency, suggesting that the decrease of the mechanical parameters with increasing porosity is mainly governed by the decrease in effective loaded volume. The two data sets of Figure 3 can be described mathematically as suggested in (6) for ceramic materials, which in turn is based on (7).

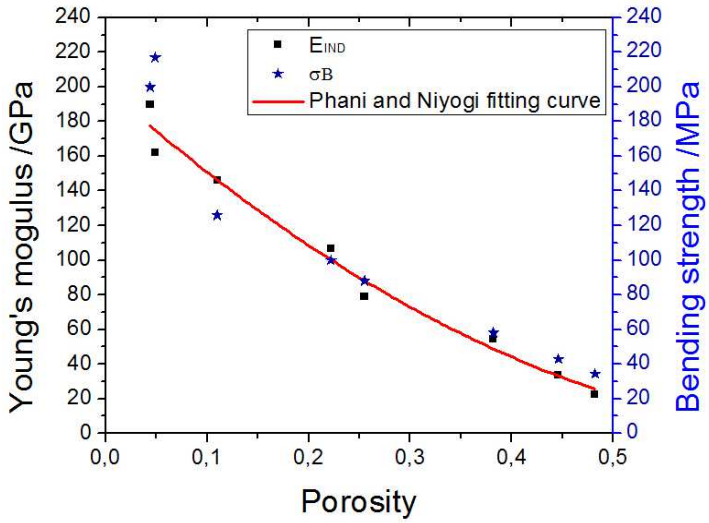

Figure 3. Porosity dependency of the Young's modulus and the bending strength (SYT only).

From this initial work (see also 5), it can be seen that the temperature dependency of the materials properties can be described by the Young's modulus. For porous materials the porosity dependency of the bending strength can be approximated by the behaviour of the Young's modulus (assuming pores are much smaller than failure relevant defects and small tortuosity). Obviously, Young's modulus and strength of a porous material will never be higher than that of the equivalent dense materials. STN94 material seems to be the most stable in the studied temperature range. TABLE II summarises some the determined mechanical properties for the three different studied systems.

TABLE II Summary of determined mechanical properties for STN, SYT and LSCT materials of this study

	SYT	**STN94**	**LSCT**
Fracture stress* **	79 MPa, tape-casting 56 MPa, warm-pressing	81 MPa, tape-casting	54 MPa, double tape-casting
Young's modulus * **	72 GPa	94 GPa	79 GPa
Porosity dependence		$E(\sigma) = E_0 \cdot (\sigma_0)(1-1.372 \cdot P)^{1.897}$	
Possible fracture origins	pore seams	dense inclusions	large voids

* Young's modulus and fracture stress values were determined via the extrapolation of the measured data to the cell-relevant porosity value (P = 0.3) with the porosity dependence listed in this table.
** Young's modulus and fracture stress values are listed for the room temperature..

Button Cell Performance

A comparison between button cell performance as area specific resistances (ASR), all equipped with LSM based cathodes and different ST-based anodes, and tested in 200 ml/min H_2, 400 ml/min air, 10 % H_2O at 900 °C can be seen in Figure 4. In comparison to a Ni/8YSZ reference, the cell with the LSCT anode showed the best performance. The cells with SYT and LST/YSZ anodes show a slightly higher ASR when compared with LSCT. However, both cells were equipped with unsintered cathodes, which can partially justify higher cell losses for these cells. As shown in Figure 1, STN materials exhibit the lowest of the measured electrical conductivity values. This fact is now considered to lead to contacting issues, due to the low in-plane conductivity, and thus would be responsible for the higher ASR.

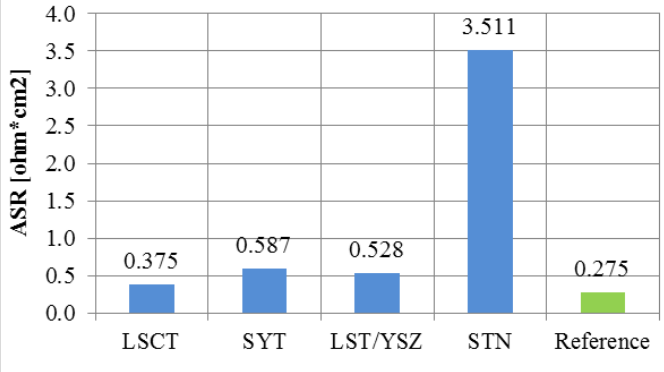

Figure 4. Comparison of cell ASR values with different ST-anodes, characterized in a Hexis button cell test rig at 900 °C, 200 ml/min H_2, 400 ml/min air, 10 % H_2O.

Benchmarking several ST-anodes in the button cell configuration has further shown that the potential contacting issue can be improved by redox-cycling, resulting in area specific resistances (ASR) of 0.3 – 0.60 Ωcm^2 (900°C) for the tested cells. This interpretation is supported by the equal scaling of both the ohmic and the polarization resistance, in addition to known low electrical conductivities of those anodes as shown before.

Figure 5 shows the impact of 20 redox-cycles and prolonged exposure of a LSCT(Ni/CeO_2 infiltrated) anode on a button cell level. The ohmic resistance (R_{ohm}) stayed constant after 20 redox cycles, verifying the excellent redox stability of this anode. Note that the ASR of the cell in Figure 5 (left) is close to the ASR of a standard cell having a Ni-Cermet anode under the same operating condition (0.38-0.43 Ωcm^2 at 850°C) after some redox-cycles. This clearly shows that the ceramic anode has the potential to replace the state-of-the-art Ni-cermet anode from a performance point of view. However, the polarization resistances (R_{pol}) of the LSCT-based anode increased significantly with time, and at higher rates than those reported for Ni-cermet anodes (Figure 5, right). This is a common feature of all ST-based anodes of this study. Current assumptions that needs further verification is that the increase of the R_{pol} is linked to the agglomeration and continuous re-distribution of the infiltrates and/or changes in properties of infiltrate-backbone interactions at the current operating conditions.

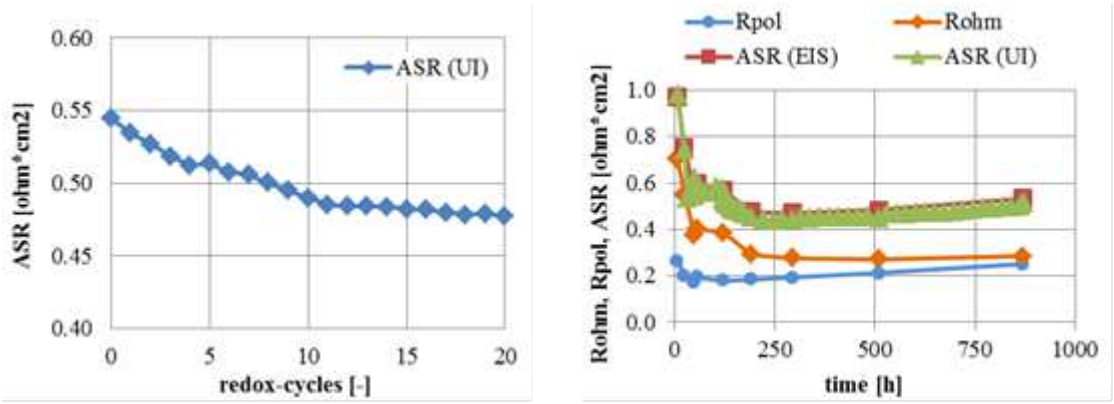

Figure 5. ASR as a function of several redox-cycles of a LSCT(Ni/CeO_2 infiltrated) anode and LSM cathode (left) and as a fuction of time (right) characterized in a Hexis button cell test rig at 850 °C, 200 ml/min H_2, 400 ml/min air, 10 % H_2O.

Full Cell Performance on a ESC Design

The initial iV-curves and performance characteristics of a cell with a Ni/CGO infiltrated composite STN94/8YSZ anode are shown in Figure 6. Further information on STN-based cells can be found in (8). At the early stages, power densities above 0.4 W/cm^2 were obtained. However, and as previously mentioned, the power output decreased significantly after the initial characterization period of less than 100 hours and a RedOx cycle, as can be seen in Figure 6. Subsequent reduction of the anode in 4 % H_2O/H_2 for 24 hours at 850 °C did not improve the anode performance, actually the power output was further decreased.

Operating the cell under methane internal reforming conditions (iR), and 60 % fuel utilization, degraded the cell rapidly, as reflected in a the 650 mV to 450 mV voltage drop in less than 12 hours. After redox-cycling the anode in technical humidified air, the iV-curve and power-output recovered to values prior to starting the internal reforming (see Figure 6). However, after returning the cell to 60 % fuel utilization under iR, the cell voltage again dropped almost instantaneously to 450 mV. This reversible performance loss might indicate a limitation of the STN cells in its internal reforming or water gas shift activity. To which extend the low Ni loading and/or Ni agglomeration accounts for this performance loss has to be analyzed further.

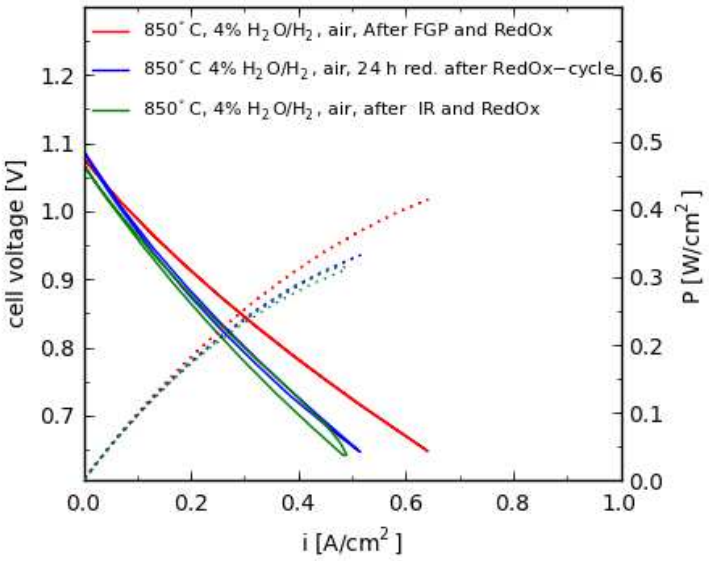

Figure 6. Cell voltage and power output as a function of time for a Ni/CGO infiltrated STN94/8YSZ anode and LSM cathode on a ESC design. , iV-curves and power-outputs are shown for after the initial RedOx following the cell characterization, 24 hours after re-reduction in 4 % H_2O/H_2 and after iR conditions, 60 % fuel utilization (269 mA/cm^2) and a second subsequent RedOx cycle. The iV-curves shown were measured at 120, 145 and 177 hours into the experiment. iV-curves are measured in 4 % H_2O/H_2 to the anode with air at the cathode.

Short-stack Testing

LSCT anodes have been further tested in a 5 cell stack based on Hexis ESC design (100 cm^2 cell area) using a Ni-mesh as current collector. The average cell performance obtained under CPOX reformed natural gas is shown in Figure 7 compared to a reference Ni-cermet based cell. Although the initial power output was slightly lower than the reference cell, no particular limitation is indicated from the iV-curve at high fuel utilization (> 80 %).

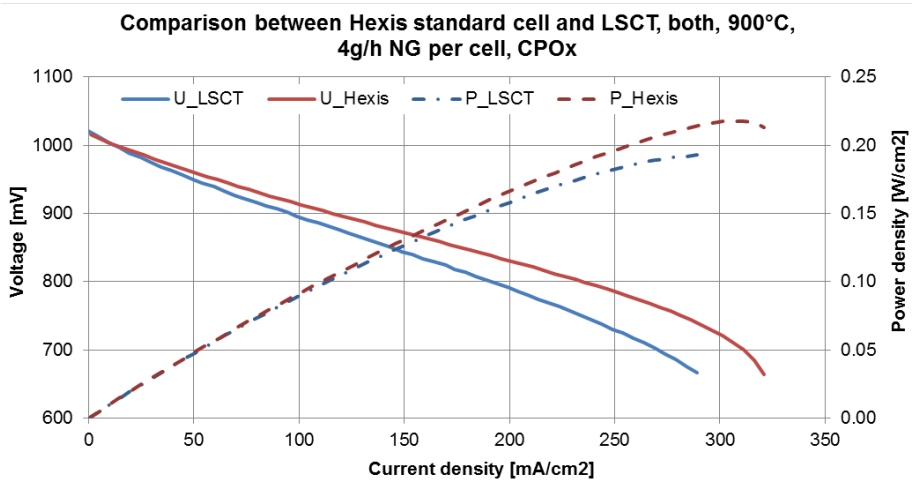

Figure 7. iV-curve and performance characteristic of an ESC with LSCT anode and LSM cathode, in comparison with a reference Ni/YSZ Hexis cell (start of experiment). A fuel utilization of 80 % is reached around 250 mA/cm^2.

Anode Supported Cell (ASC) Development

The status of ASC development is summarized in TABLE III. Co-sintering of the electrolyte layer and support, as well as brittleness of the support itself, have been identified as major problems in this cell design when upscaling to 144 cm^2 sized cells.

TABLE III. Overview of current developments on the anode supported desing

	LSCT	**SYT**	**STN**
Support dimensions	5 x 5 cm^2	5x5 cm^2 14 x14 cm^2	14x14 cm^2
Cell integration	On-going	Achieved	Co-sintering issues
Handling of cells	-	brittle	brittle
Performance testing	Button cells	Up to 5x 5 cm^2	-

ASCs based on SYT and LSCT have been electrochemically tested on 25 cm^2 and 1 cm^2 cells, respectively. The cell tests on SYT based ASCs with Ni/CGO infiltration showed initial ASRs between 0.4 and 0.7 Ωcm^2. The power output was 0.3 Ωcm^2 at 0.7 V cell voltage. It should be noted that the OCV was significantly lower than the theoretical but the reason has not yet been fully identified. Interdiffusion of Ti into the YSZ electrolyte is known to occur and could introduce some level of electronic conductivity into the electrolyte. The measured oxygen increase in the fuel compartment is, however, rather high assuming an oxygen ion flux through the mixed conducting electrolyte. The lower OCV might explain why the performance is lower than previously reported (9). First stacking of 144 cm^2 cells points to residual stresses in the support, and thus gas leakages due to electrolyte cracking cannot be excluded for these cells.

LSCT-based ASCs have been tested as button cells only in 3 % H_2O/H_2, with and without infiltration. Interestingly, the LSCT material itself revealed already some activity for hydrogen oxidation. With impregnated Ni/CGO as electro-catalysts, initial power outputs of 1 W cm^2 have been achieved (10)

Long-term Stability

The time dependence of the cell performance was tested, for the three different ST-systems, up to several hundreds of hours, under constant current load and high steam content to assess anode stability.. At temperatures above 850 °C, all cells significantly degraded and an overview is provided in TABLE IV.

TABLE IV. Overview of degradation rates observed for the three different ST systems

	LSCT	**YST**	**STN**	**Ni-Cermet reference**
Voltage degradation [mV/kh]	400	175	375-500	3.5
Cell geometry	5 cell stack	25 cm^2 cell	25cm^2	100 cm^2
Test conditions	CPOX 80% fuel utilization	4% H_2 in H_2O	H_2 / 50% steam	CPOX
Temperature [°C]	950	850	850	900
Infiltrate	Ni/CeO_2	Ni	Ni-CGO	None
Comment	--	Possible leaks or electronic short-circuit through the electrolyte	--	

As shown already in Figure 5 the degradation is generally related to a decrease in R_{pol}, thus related to the electrochemical activity of the electrodes, while R_{ohm} remains constant. Infiltrate agglomeration and Ni particle growth have been observed for all samples, however, these modifications seem to dependent on testing time and conditions. To date, and as previously mentioned, it remains to be answered if the high measured degradation rates have one or several factors, all involving the infiltrates, at the testing conditions, namely the morphological and/or chemical alterations of the infiltrates or of the nature of the infiltrates-backbone characteristics.

TABLE V. Overall evaluation of the three main ST-systems of this study.

Property	**LSCT**	**YST**	**STN**
Conductivity	+	O(only prereduced tested)	O
Mechanical strength	O	O	(+)
Redox stability	+	+	+
EC performance	+	+	+
Durability	--	-	--

Symbol indications: + (good), O (indifferent/ medium), - (problematic)

Conclusions

In this study, three ST-based materials have been characterized and integrated into electrolyte and anode supported cell designs. TABLE V summarizes the important parameters to take into account in the evaluation of their potential as SOFC anodes. From their chemical, electronic and mechanical properties, all three materials are in principle applicable as anodes and anode supports. Satisfactory electrochemical performance is obtained by infiltration with electro catalysts such as Ni and CGO or a combination of

both. The stability of the infiltrated catalysts has been identified as a performance limitation at temperatures of 850 °C and above, limiting their application in electrolyte supported cell designs.

With respect to the development of anode supported cells, promising initial cell performances have been obtained. However, electrical conductivity and mechanical strength are still lower than expected, which can tentatively be justified by the further need for processing optimization of ST-based materials.

In conclusion, ceramic SOFCs based on strontium titanates can be manufactured and tested at technical dimensions (100 cm^2 area), including in short-stacks. In this type of cell, porous strontium titanate acts as a support for electro active catalysts. Thus, the concepts opens up the use of other catalytically active materials, allowing the tailoring of anode properties with respect to sulfur and coking tolerance.

Acknowledgments

The research leading to these results has received funding from the European Union's Seventh Framework Programme (FP7/2007-2013) for the Fuel Cells and Hydrogen Joint Technology Initiative under grant agreement no. 256730.

The authors would like to thank Karsten Agersted. Peter Stanley Jørgensen, Wei Zhang, and Janet Jona Bentzen for microstructure analysis.

References

1. P. Holtappels. and B.R. Sudireddy, *Chapter 9 Ceramic Fuel Cells, in Ceramic Science & Technology Vol. 4 Fuel Cells*, Wiley VCH, (in press) (2013).
2. K. Agersted, P. Holtappels, J. T. S Irvine, Q. Mac, J. Malzbender, T. Ramos, F. Tietz and M.V. Verbraeken, *Review on Sr-Ti electrodes, SCOTAS-SOFC public report* D3.01 (in preparation).
3 L. Baque, S. Jørgensen, K. V. Hansen and M. Søgaard, *ECS Trans*., These proceedings
4. P. Vozdecky, A. Roosen, Q. Ma, F. Tietz and H.P. Buchkremer, *J. Mater. Sci.,* **46**, 3493 (2011).
5. B.X. Huang, V. Vasechko, Q.L. Ma and J. Malzbender, *Journal Power Sources*, **206**, 204 (2011).
6. Y. Yao, *Master thesis*, RWTH Aachen, (2012).
7. K.K. Phani and S.K. Niyogi, *J. Mater. Sci.*, **32**, 257 (1987), pp -263.
8. B.R. Sudireddy, S. Veltzé, P.S. Jørgensen, L. Theil Kuhn, P. Holtappels and T. Ramos, *ECS Trans*., These proceedings.
9 Q. Ma, F. Tietz, A. Leonide, and E. Iver-Tiffee, *J. Power Sources*, **196** , 7308 (2011).
10. L.Y. Lu, M.C. Verbraeken, M. Cassidy, and J.T.S. Irvine, *ECS Trans*., These proceedings.